

Supplementary Information

Graphitic edge plane rich meso-porous carbon anode for alkaline water electrolysis

Dongyoon Shin,^{a,b} Myounghoon Choun,^{a,b} Hyung Chul Ham,^c Jaekwang Lee,^{b,d} and

*Jaeyoung Lee^{*a,b,d}*

^a Electrochemical Reaction and Technology Laboratory (ERTL), School of Environmental Science and Engineering, Gwangju Institute of Science and Technology (GIST), Gwangju 500-712, Republic of Korea

^b Ertl Center for Electrochemistry and Catalysis, GIST Research Institute, GIST, Gwangju 500-712, Republic of Korea

^c Fuel Cell Research Center, Korea Institute of Science and Technology (KIST), Seoul 136-791, Republic of Korea

^d Chemical Energy Storage and Transformation Center, RISE, GIST, Gwangju 500-712, Republic of Korea.

* Corresponding Author

E-mail: jaeyoung@gist.ac.kr, Tel: +82 62 715 2440

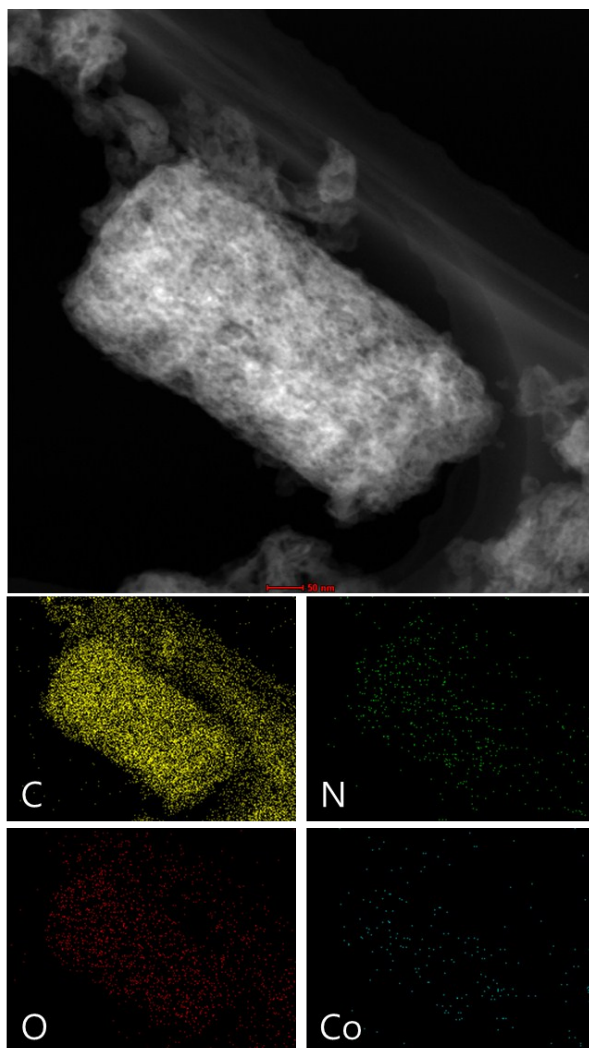


Figure S1. STEM image of A-Co-N-CNF and elemental mapping images.

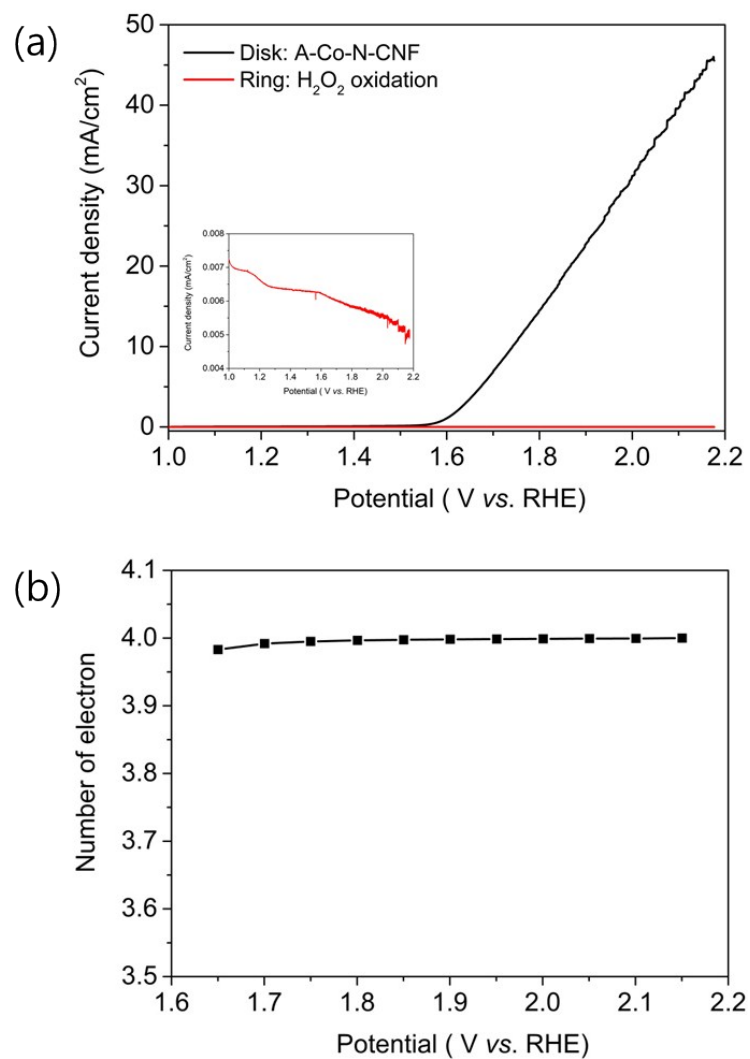


Figure S2. (a) Rotating ring disk electrode measurements for detection of H₂O₂ generated from the A-Co-N-CNF catalysts. (b) The number of electrons calculated from the rotating ring disk electrode measurement (ring potential: 1.5 V vs. RHE).

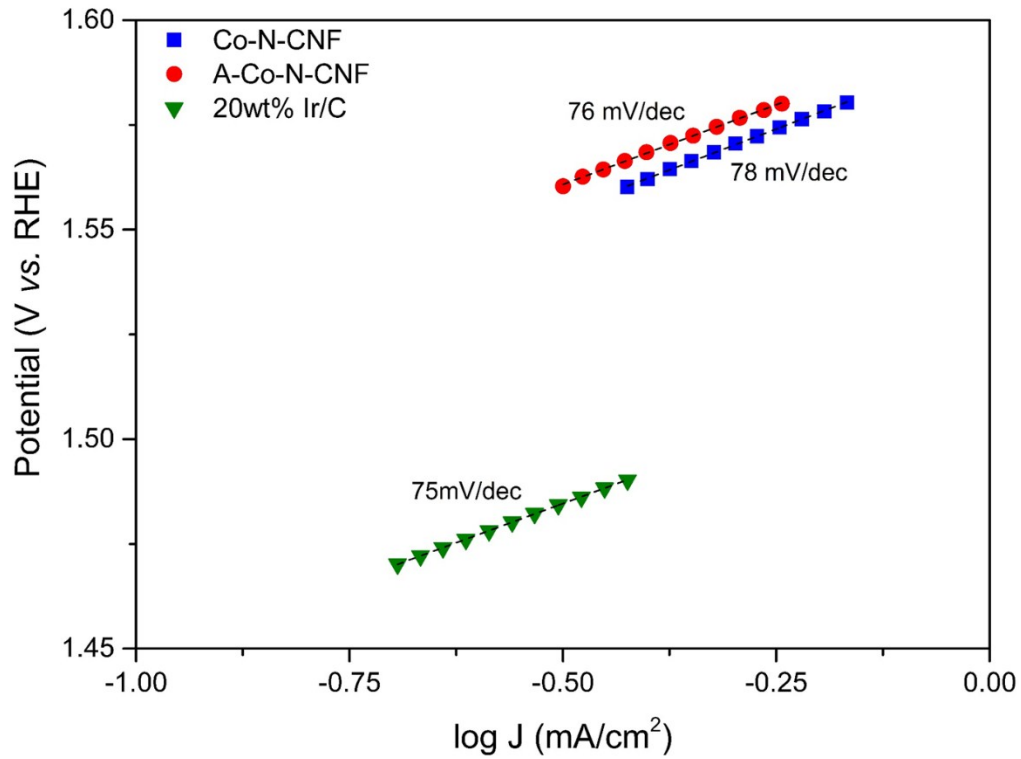


Figure S3. Tafel plots for Co-N-CNF, A-Co-N-CNF, and 20 wt% Ir/C which are obtained from linear sweep voltammetry at a scan rate of 5 mV s⁻¹ (not iR-Corrected).

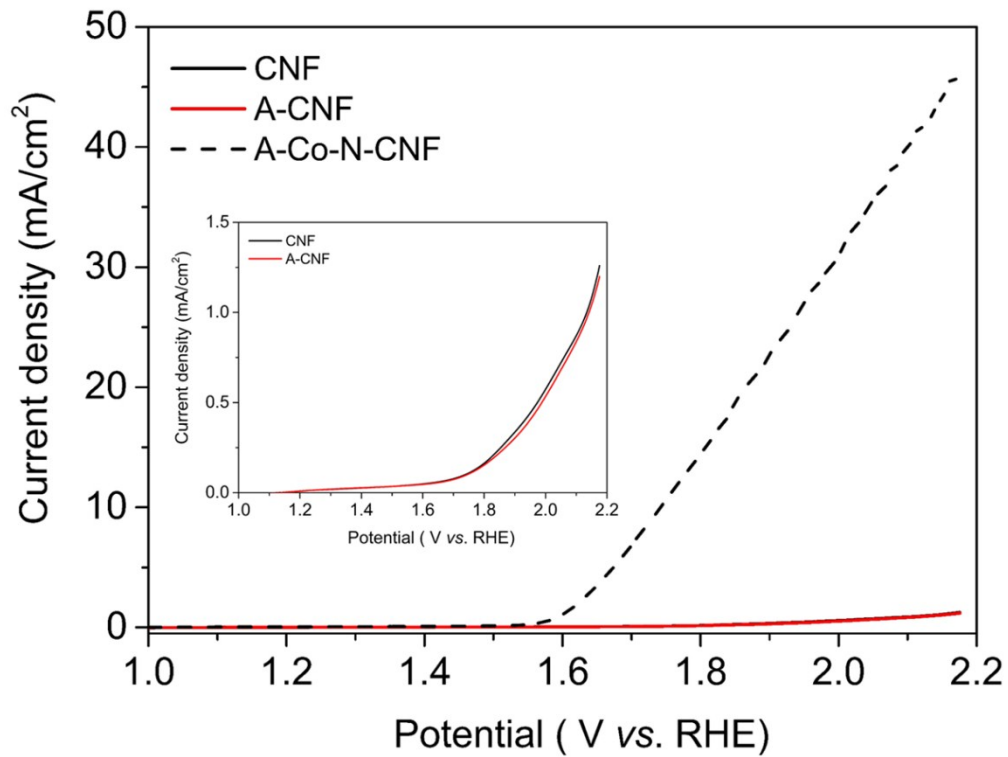


Figure S4. Oxygen evolution reaction activity of A-Co-N-CNF, CNF, and A-CNF with rotating disk electrode at a rotating rate of 1600rpm and a scan rate of 5 mV s⁻¹ in N₂-saturated 0.1 M KOH aqueous solution.

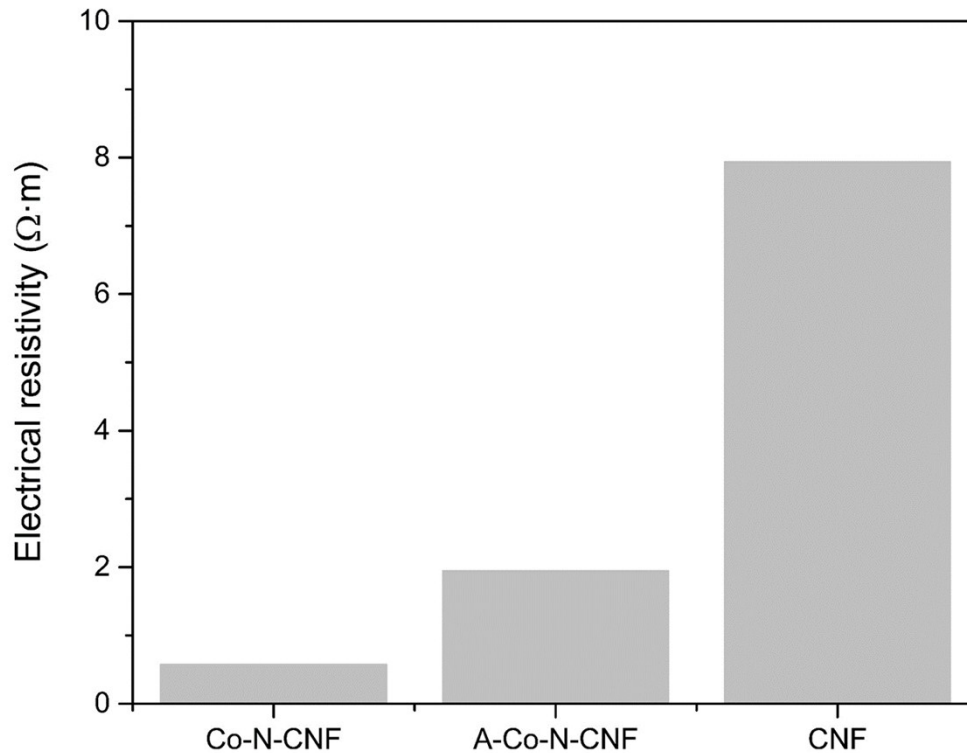


Figure S5. The results of electrical resistivity measurement by four-point probe for Co-N-CNF, A-Co-N-CNF, and CNF. Each sample was coated on carbon paper, where thickness was 300 μm and the probe thickness was 1.590 mm. For accurate reliability, each test was conducted on 3 different samples and repeated at least 20 times.

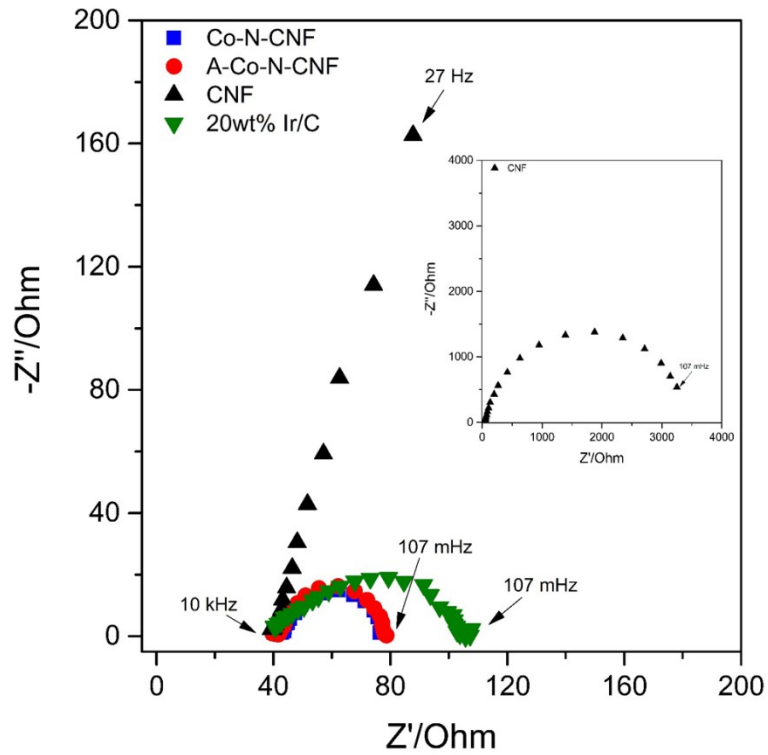


Figure S6. Nyquist plots obtained by EIS at 450 mV overpotential for the oxygen evolution reaction. The frequency range investigated reached from 10 kHz to 107 mHz with 30 points.

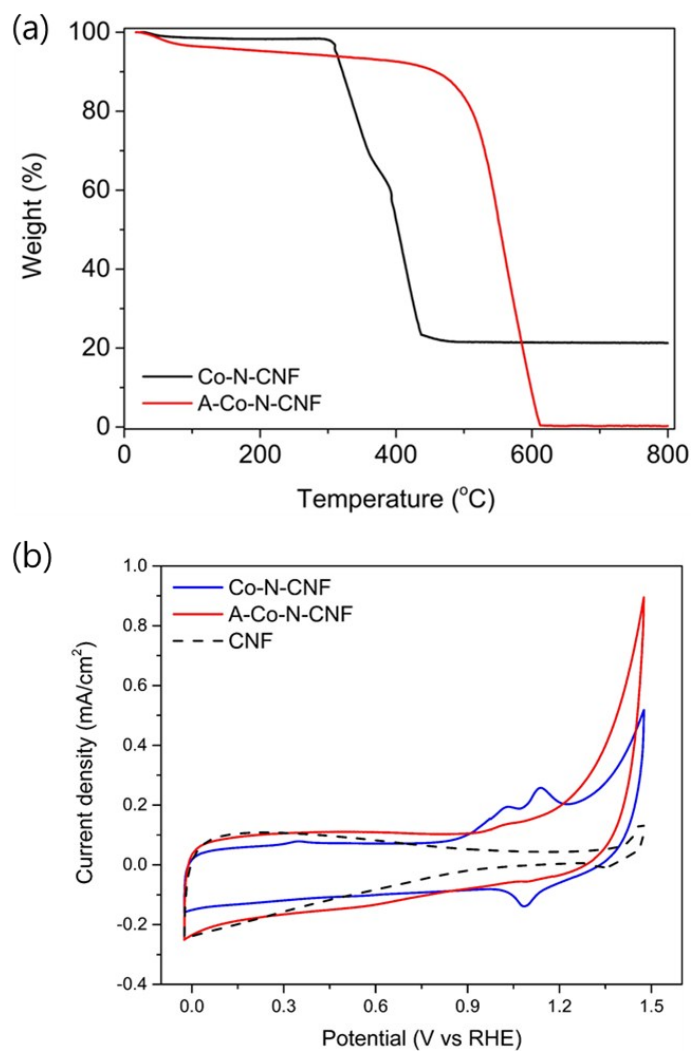


Figure S7. (a) Thermo-gravimetric analysis of Co-N-CNF and A-Co-N-CNF under air environment, (b) Cyclic voltammograms of Co-N-CNF, A-Co-N-CNF, and CNF in N_2 -saturated 0.1 M KOH aqueous solution with glassy carbon electrode at a scan rate of 5 mV s^{-1} .

Table S1. The bulk element composition of Co-N-CNF, A-Co-N-CNF, and CNF (wt%). The composition of metal is obtained from thermo-gravimetric analysis and the composition of C, N, and O is measured by energy dispersive spectrometer.

Sample	C	N	O	Co
Co-N-CNF	76.77	0.76	1.20	21.27
A-Co-N-CNF	96.94	0.44	3.62	-
CNF	94.43	2.23	3.34	-

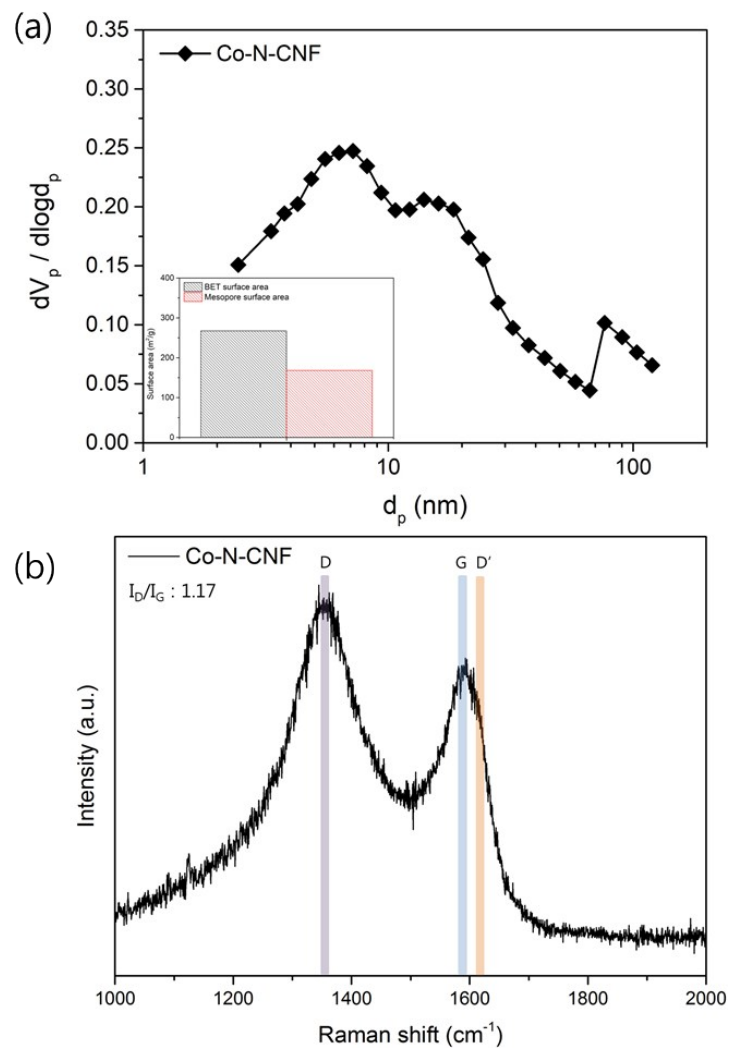


Figure S8. (a) Pore size distribution and (b) Raman spectrum of Co-N-CNF. The inset indicates the BET surface area and mesopore surface area.

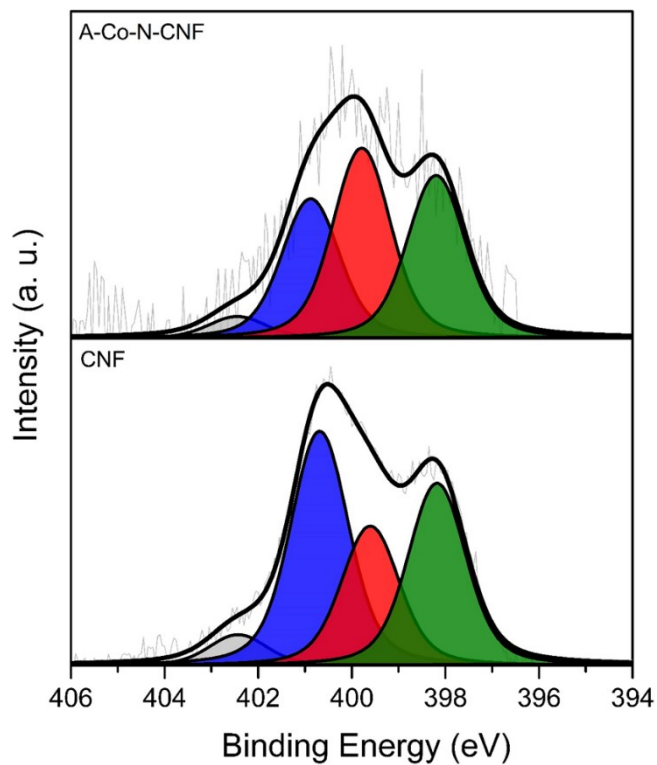


Figure S9. X-ray photoelectron spectrum at N 1s of A-Co-N-CNF and CNF. Each line denotes the various binding energies of doped nitrogen: Pyridinic-N; ~398 eV, Pyrrolic-N; ~400 eV, Graphitic-N; ~401 eV, and Pyridinic-N-oxide; 402–403 eV.

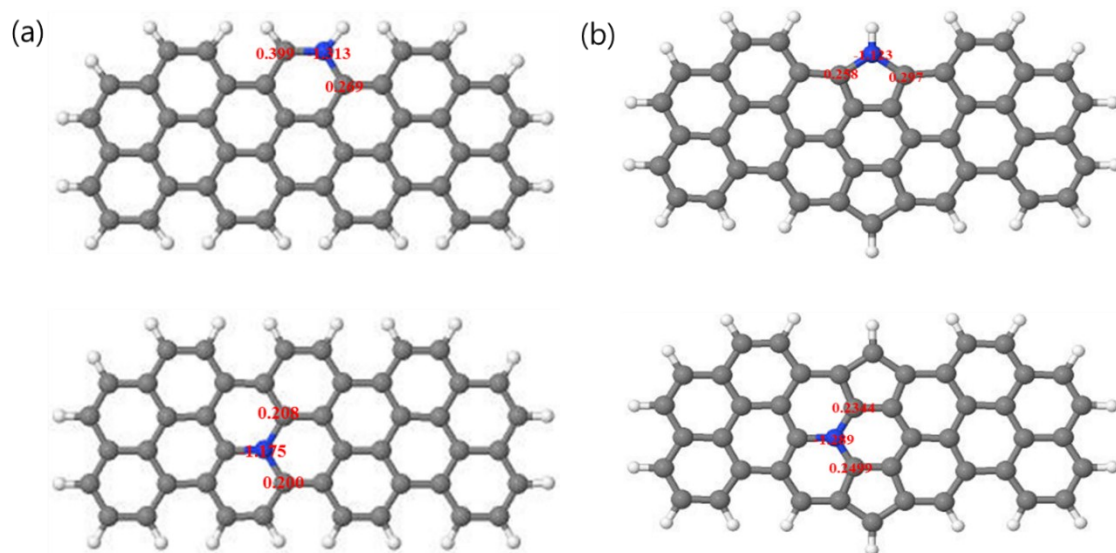


Figure S10. Partial charge distributions of nitrogen-doped graphite surfaces with different doping position. (a) (upper) $C_{45}N(\text{edge})H_{20}$, (lower) $C_{45}N(\text{basal})H_{20}$ and (b) (upper) $C_{45}N(\text{edge})$, (lower) $H_{18} C_{45}N(\text{basal})H_{18}$. Gray; carbon atoms, blue; nitrogen atom, white; hydrogen atoms. The charge distributions are shown in Table S2.

Table S2. Partial charge distributions of nitrogen-doped graphite surfaces with different doping position. The negative sign indicates the electronic charge gain and all values are given in e unit.

(a)	Charge distribution for $C_{45}N(\text{edge})H_{20}$,	Charge distribution for $C_{45}N(\text{basal})H_{20}$
N	-1.314	-1.175
C1	0.399	0.314
C2	0.269	0.208
C3	0.057	0.143
C4	0.062	-0.008
Average charge distribution of carbon atoms near a N atom	0.197	0.164

(b)	Charge distribution for $C_{45}N(\text{edge})H_{18}$	Charge distribution for $C_{45}N(\text{basal})H_{18}$
N	-1.123	-1.351
C1	0.258	0.214
C2	0.297	0.363
C3	-0.004	0.274
C4	0.036	0.113
C5	N/A	0.004
C6	N/A	-0.098
Average charge distribution of carbon atoms near a N atom	0.147	0.145

*** Computational details:**

The calculations reported herein were performed on the basis of spin-polarized density functional theory (DFT) within the generalized gradient approximation (GGA-PBE¹), as implemented in the Vienna Ab-initio Simulation Package (VASP²). The projector augmented wave (PAW) method with a planewave basis set was employed to describe the interaction between ion cores and valence electrons³. The PAW method is in principle an all-electron frozen-core approach that considers exact valence wave functions. An energy cutoff of 400 eV was applied for the plane-wave expansion of the electronic eigenfunctions. In this study, we considered four different nitrogen-containing graphene clusters: (I) C₄₅N(edge)H₂₀, in which a N atom is located in the edge of graphene cluster, (II) C₄₅N(basal)H₂₀, in which a N atom is located in the basal of cluster, (III) C₄₅N(edge)H₁₈, in which a N atom is located in the edge of graphene cluster, (IV) C₄₅N(basal)H₁₈, in which a N atom is located in the basal of graphene cluster. Here, the configuration of N atoms in each edge and basal location is determined by comparing the total energy of different N positions in graphene clusters. For the edge case, the configuration of H-terminated N atom is chosen since that is more energetically stable by 0.29eV(C₄₅NH₂₀) and 0.20eV (C₄₅NH₁₈) than the bare N atom case. For the basal case, the configuration of N atoms directly connected to the edge carbon is calculated to be more stable by 0.01eV(C₄₅NH₂₀) and 0.72eV(C₄₅NH₁₈) than the configuration of N atoms bonded to the basal carbon.

All atoms in graphene clusters were fully relaxed using the conjugate gradient method until residual forces on all the constituent atoms become smaller than 5×10^{-2} eV/Å. For Brillouin zone integration, we used one k-point (Gamma point) with graphene clusters in a

periodic box of dimension = $30 \times 30 \times 20$ Å. We further checked the convergence of our calculation results with respect to different k-point mesh size, indicating that the chosen values are sufficient for describing the total energies of the model systems considered. We evaluated the atomic charge states of nitrogen-containing graphene clusters using the Bader method⁴ with the optimal convergence with respect to charge density grid.

Reference

- (1) Perdew, J. P.; Burke, K.; Ernzerhof, M. *Phys. Rev. Lett.* **1996**, *77* (18), 3865–3868.
- (2) Kresse, G.; Furthmüller, J. VASP the Guide; Vienna University of Technology: Vienna, Austria, 2001.
- (3) Blöchl, P. E. *Phys. Rev. B* **1994**, *50* (24), 17953–17979.
- (4) Sanville, E.; Kenny, S. D.; Smith, R.; Henkelman, G. *J. Comput. Chem.* **2007**, *28* (5), 899–908.